Article

Cell Reports

# Rhythmic Degradation Explains and Unifies Circadian Transcriptome and Proteome Data

## Graphical Abstract

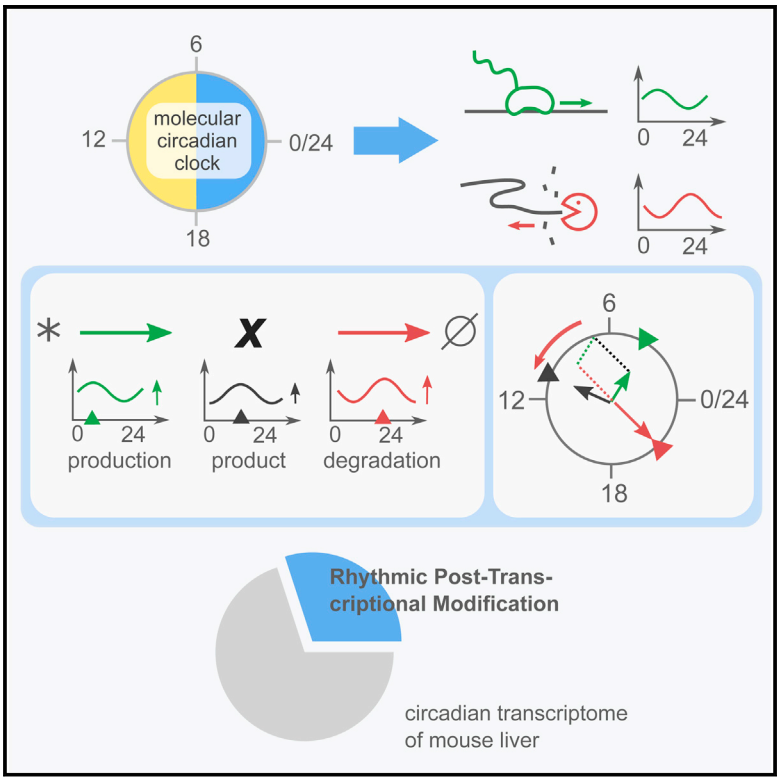


## Authors

Sarah Lück, Kevin Thurley, Paul F. Thaben, Pål O. Westermark

## Correspondence

pal-olof.westermark@charite.de

## In Brief

Lück et al. show how circadian variations in half-lives affect abundances of mRNAs and proteins. After developing a statistical test for detecting rhythmic posttranscriptional regulation, the authors go on to show that at least 30% of circadian transcripts in mouse and fly are affected. They further demonstrate a "curse of mean half-lives": the mean half-life of an mRNA or protein always must lie below 50 hr for rhythms to persist, regardless of how the rhythms are generated.

## Highlights

The circadian clock affects both production and degradation of mRNAs and proteins

A phase vector model explains effects of rhythmic degradation

Rhythmic degradation causes nontrivial effects such as magnitude amplification

Rhythmic posttranscriptional regulation affects 30% of circadian transcripts

Lück et al., 2014, Cell Reports 9, 741–751
October 23, 2014 ©2014 The Authors
http://dx.doi.org/10.1016/j.celrep.2014.09.021

Cell Reports
Article



# Rhythmic Degradation Explains and Unifies Circadian Transcriptome and Proteome Data

Sarah Lück,[1,2] Kevin Thurley,[1,2] Paul F. Thaben,[1] and Pål O. Westermark[1,*]
[1]Institute for Theoretical Biology, Charité—Universitätsmedizin, 10115 Berlin, Germany
[2]Co-first author
*Correspondence: pal-olof.westermark@charite.de
http://dx.doi.org/10.1016/j.celrep.2014.09.021


## SUMMARY

**The rich mammalian cellular circadian output affects thousands of genes in many cell types and has been the subject of genome-wide transcriptome and proteome studies. The results have been enigmatic because transcript peak abundances do not always follow the peaks of gene-expression activity in time. We posited that circadian degradation of mRNAs and proteins plays a pivotal role in setting their peak times. To establish guiding principles, we derived a theoretical framework that fully describes the amplitudes and phases of biomolecules with circadian half-lives. We were able to explain the circadian transcriptome and proteome studies with the same unifying theory, including cases in which transcripts or proteins appeared before the onset of increased production rates. Furthermore, we estimate that 30% of the circadian transcripts in mouse liver and *Drosophila* heads are affected by rhythmic posttranscriptional regulation.**

## INTRODUCTION

Circadian rhythms in mammalian cells control a wide range of cellular processes. These rhythms arise in genetic feedback loops, which consist of clock genes that code for clock proteins. Some of the clock proteins are transcription factors and transcriptional coregulators that repress or activate their own expression or that of other clock proteins, forming a small network of feedback loops that is viewed as the core cellular circadian clock (Zhang and Kay, 2010). A rich circadian output is thought to arise partly through circadian transcriptional regulation by clock transcription factors and coregulators, whose target genes are termed clock-controlled genes (Doherty and Kay, 2010; Asher and Schibler, 2011). Even more genes are rhythmically expressed due to external circadian signaling to the cell (e.g., circadian hormonal signaling), which affects many cell types (Asher and Schibler, 2011). In mouse liver, for instance, there are circadian rhythms in the mRNA expression of thousands of genes (Hughes et al., 2009), and the charting of how these rhythms orchestrate diverse cellular processes is an active research area. For example, many aspects of metabolism (Asher and Schibler, 2011; Bass and Takahashi, 2010), as well as the cell cycle (Matsuo et al., 2003), are regulated by the circadian clock.

While the mechanism of the core circadian clock is understood in some detail, the processes that govern the circadian output are not as well characterized. However, it is clear that both transcriptional and posttranscriptional mechanisms are at work (Kojima et al., 2011; Doherty and Kay, 2012). Investigations into the circadian regulation of intracellular processes are challenged by the difficulty of separating transcriptional effects from posttranscriptional regulation. Rhythmic mRNA abundance may be caused by rhythmic transcriptional activity, rhythmic regulation of mRNA half-life, or a combination of these processes. Similarly, rhythmic protein abundance may be caused by both rhythmic translational activity (often due to rhythmic mRNA abundance) and rhythmic protein half-life. It is not understood how a combination of rhythmic production and degradation affects the oscillation amplitude and phase (peak time) in the abundance of a regulated biomolecule, challenging the interpretation of experimental results.

There are many examples of circadian rhythmicity in regulators of mRNA and protein stability. These include rhythmic poly(A) tail lengths (Robinson et al., 1988; Baggs and Green, 2003; Kojima et al., 2012), abundances of RNA-binding proteins (Liu et al., 2013; Morf et al., 2012; Woo et al., 2010), and miRNAs (Vollmers et al., 2012). The activity of autophagy, one of the major protein degradation pathways in the cell, is circadian in mouse liver (Ma et al., 2011). Moreover, strong evidence for posttranslational circadian regulation comes from proteome-wide studies of circadian rhythms in protein abundances (Mauvoisin et al., 2014; Reddy et al., 2006; Robles et al., 2014). The circadian phases of rhythmic proteins are often distinct from the phases of the transcripts; for example, protein abundance can peak a few hours before mRNA abundance (Reddy et al., 2006). This cannot be explained without additional mechanisms, as biochemical kinetics dictates that the abundance of a rhythmically produced molecule with a constant half-life will peak between 0 and 6 hr after the peak in production rate. Recent high-throughput studies of the circadian transcriptome in mouse liver and *Drosophila* heads raised similar questions (Koike et al., 2012; Le Martelot et al., 2012; Menet et al., 2012; Rodriguez et al., 2013), since the phase of circadian transcriptional activity is often a poor predictor of the phase of the mature transcript abundance.

In this report, we show that such observations can be completely explained by assuming rhythmic degradation in

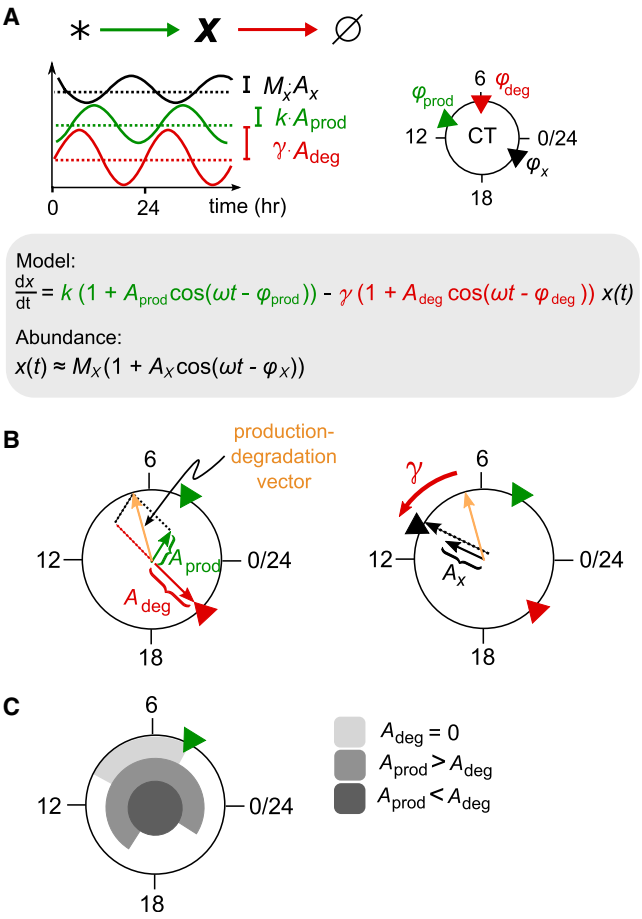


**Figure 1. Phase Vectors Reveal Phase and Amplitude Relationships**

(A) Model. A molecule $x$ is produced and degraded with rate coefficients that periodically change with the circadian frequency $\omega = 2\pi/24\ hr^{-1}$. In the model equation, the production rate coefficient is marked in green and the degradation rate coefficient is in red. $k$ and $\gamma$ are the mean rate coefficients, which experience a time modulation described by cosine-shaped functions with relative (percentage) amplitudes $A_{prod}$ and $A_{deg}$ (values between 0 and 1), and the phases $\varphi_{prod}$ and $\varphi_{deg}$. Here, the phases are represented in circadian time (CT) but have the unit radians in all equations. The abundance of $x$ is described by its magnitude (mean) $M_x$, relative amplitude $A_x$, and phase $\varphi_x$.

(B) The analytical approximation (Experimental Procedures) describes $A_x$ and $\varphi_x$ as a vector difference (see Equation 1): $A_{prod}$, $\varphi_{prod}$ and $A_{deg}$, $\varphi_{deg}$ are represented by the lengths and angles of vectors in the circadian plane. The vector difference between production and degradation is formed to obtain a production-degradation vector (left circle). This vector is rotated by a half-life-dependent phase lag (rounded arrow and Equation 1) and scaled by a half-life-dependent factor (Equation 2). The resulting vector represents the phase and, save for a correction factor $C$, the relative amplitude of $x$ (right circle, see Experimental Procedures).

(C) Range for the phase $\varphi_x$ given a certain production phase (green arrow), depending on the ranges of the relative amplitudes. The actual phase within this range also depends on the mean half-life and degradation phase.

See also Figure S1.

addition to rhythmic production. To this end, we derived a unifying theoretical framework and developed methods that provide a comprehensive understanding of the dynamics of rhythmically produced and rhythmically degraded molecules of any kind, such as mRNAs and proteins. We show that the mean half-life of a molecule is critical for significant rhythmicity and derive analytical expressions for the amplitude, phase, and magnitude in the abundance of a rhythmically degraded molecule. We developed a freely available accompanying software package designed to detect posttranscriptional rhythmic regulation in genome-wide data sets. We then applied our tools to the genome-wide data produced in studies by Menet et al. (2012) and Rodriguez et al. (2013), and were able to quantify the extent of rhythmic posttranscriptional regulation. In particular, we show that rhythmic half-lives provide a possible explanation for the observed large phase differences between transcriptional activity and mature mRNAs (Doherty and Kay, 2012), and between mRNAs and proteins (Reddy et al., 2006), and present evidence to support this notion.

## RESULTS

### The Phase Can Vary Arbitrarily if Production and Degradation Are Rhythmic

If a molecule is rhythmically produced but degraded with a constant degradation rate, it is intuitively clear that the abundance of the molecule will have a later phase than the production rate. However, if degradation is also rhythmic, the phase and amplitude of the molecule will depend on the phases, amplitudes, and magnitudes (average rate coefficients) of both production and degradation. Intuition can be misled by this complexity, and thus a quantitative formulation and analysis are needed. We analyzed a simple mathematical model (Figures 1A and S1A; Experimental Procedures) that describes the temporal concentration profile of a given biomolecule being produced and degraded with circadian rates, where the production and degradation rate coefficients are modeled as time-dependent, cosine-shaped functions (Figure 1A). We derived simple and accurate expressions for phases, amplitudes, and magnitudes by substituting a truncated Fourier series into $x(t)$ and neglecting small terms (Supplemental Experimental Procedures). Then, we approximated the abundance $x(t)$ by a cosine-shaped function (Figure 1A). Moreover, we found an intuitive vector representation for the phase relationships (Figure 1B): rhythmic production, degradation, and abundance of the molecule are represented by a vector in the circadian phase plane, where the angle of the vector represents the phase and its length represents the amplitude.

We found that the phase of the molecule is determined by the vector difference of the phases and amplitudes of production and degradation rate coefficients (Figure 1B, left panel, "production-degradation vector"). Furthermore, we found that the phase obtained by this vector difference must be shifted by a term depending on the average half-life to obtain a good approximation of the phase of the molecule (Figure 1B, right panel). In mathematical terms, this leads to the following equation (see Supplemental Experimental Procedures as well)

$$\varphi_x \approx \underbrace{\arg\left(A_{prod}e^{i\varphi_{prod}} - A_{deg}e^{i\varphi_{deg}}\right)}_{\text{production-degradation vector phase}} + \underbrace{\arctan\left(\frac{\omega}{\gamma}\right)}_{\text{phase shift determined by mean half-life}}, \quad \text{(Equation 1)}$$

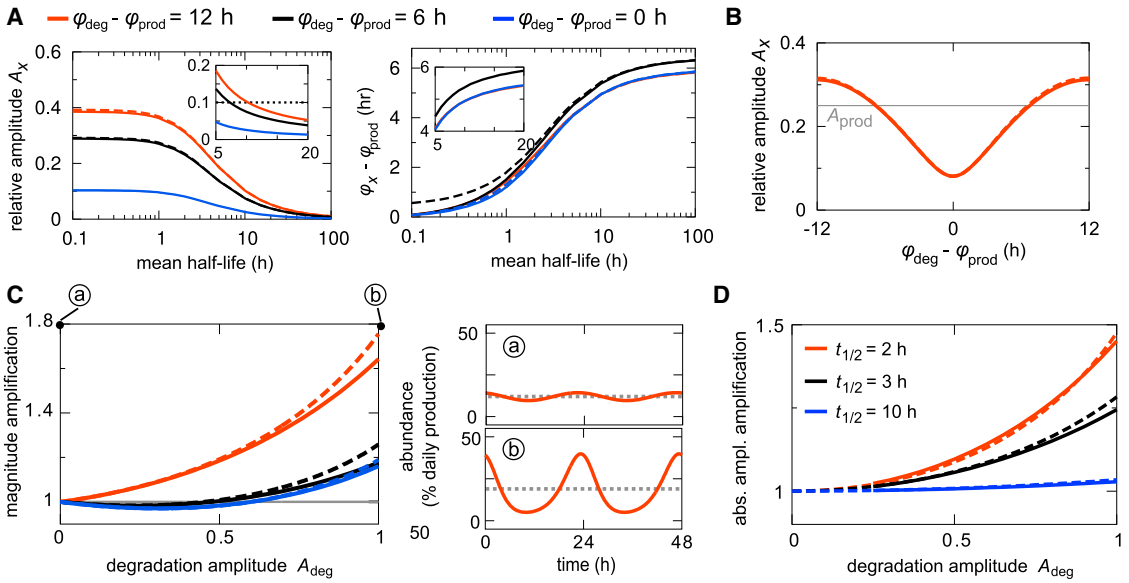


**Figure 2. Rhythmic Degradation Shapes Amplitude and Magnitude**

(A–C) Solid lines are numerical solutions of the model (Figure 1A) and dashed lines are calculated from the analytical approximations unless otherwise stated. Parameter values (if applicable): $A_{prod}$ = 0.25, $A_{deg}$ = 0.15, $k$ = 1 hr$^{-1}$, $t_{1/2}$ = 2 hr (Equations 1–3).

(A) Dependence of relative amplitudes and phases on the half-life. The dotted line in the inset indicates a postulated threshold for the significance of oscillations.

(B) The relative amplitude increases with the phase difference and with production and degradation amplitudes, but is bounded by a value smaller than $A_{prod}$ + $A_{deg}$. The gray line indicates $A_{prod}$.

(C) Magnitude $M_x$ compared with the corresponding value at constant degradation. The color key is the same as in (A). Time courses are scaled by 100/($k$ × 24 hr) to show % of daily production. The gray solid line indicates points without magnitude amplification ($M_x = k/\gamma$). Dashed gray lines in time courses are numerically calculated magnitudes.

(D) Absolute amplitude $M_xA_x$ compared with corresponding value at constant degradation. Dashed lines show only the amplification factor $2(\gamma^2+\omega^2)/(2(\gamma^2+\omega^2)-\gamma^2A_{deg}^2)$ (see Experimental Procedures). In the numerical solutions, the input amplitude was kept constant, $|A_{prod}e^{i\varphi_{prod}} - A_{deg}e^{i\varphi_{deg}}|$ = 0.25, by choosing $\varphi_{prod} = \varphi_{deg}$.

See also Figure S2.

where all symbols are as described in Figure 1. Note that the mean degradation rate coefficient $\gamma$ is related to the average half-life by $t_{1/2}$ = (ln 2)/$\gamma$. When both degradation and production are rhythmic, their relative amplitudes as well as their phases determine the production-degradation vector and therefore the phase of a molecule. In particular, if the phases of degradation and production are similar, small changes in the relative production and degradation amplitudes can cause dramatic changes in phase of up to ±12 hr. We found a simple general formula that describes this sensitivity of the phase to changes in the relative amplitudes (Supplemental Results; Figure S1B).

Another conclusion that can be drawn from Equation 1 is that phases that occur 6–12 hr earlier than the production phase can only be reached if the degradation rhythm dominates (Figure 1C). For example, if translation follows the mRNA phase, a protein appearing 6–12 hr before the mRNA would strongly suggest rhythmic degradation. Such mRNA-protein phase relationships have been observed in mouse liver (Reddy et al., 2006). When only the degradation rate coefficient is rhythmic, the phase of the molecule is fully confined to the phase interval between 12 and 6 hr earlier than the phase of the degradation rate coefficient, and the degradation rate coefficient amplitude will have no effect on the phase of the molecule.

## Long Mean Half-Lives Imply Vanishing Amplitudes

When the mean half-life is long, oscillations are always lost. This is well known in the case of constant degradation, but we found that it still holds true if the half-life is rhythmic, no matter how wildly it oscillates around its mean, and independently of all other parameters. This result can be obtained directly from the structure of the simple model by so-called scaling analysis, independently of the approximated solutions (Supplemental Results), as illustrated in Figure 2A. The relative amplitude decreases rapidly for mean half-lives longer than ~1 hr, regardless of the degradation and production phases. The phase of the rhythmically degraded molecule is shifted up to ~6 hr by long mean half-lives. However, such long phase lags always coincide with vanishing amplitudes, so that in practice, only phase shifts <6 hr can be realized by increasing the mean half-life.

It is often difficult to detect small amplitudes in practice, since they drown in both technical and biological noise, and can also hardly be expected to have important biological functions. Based on the model, we estimated maximal and typical mean half-lives that would permit generation of more readily observable relative amplitudes larger than 0.1 (Figure 1B, inset). We found that only molecules with mean half-lives shorter than 50 hr are candidates (Figure S2A). A more marked relative

amplitude of 0.25 can only be achieved with a mean half-life of <10 hr (Figure S2A).

These limits can be compared with recent transcriptome- and proteome-scale analyses indicating mean mRNA half-lives between 6 min and 50 hr and mean protein half-lives between <1 hr and 1,000 hr (Friedel et al., 2009; Schwanhäusser et al., 2011; Eden et al., 2011). Thus, most transcripts have the potential for circadian rhythmicity, whereas the half-lives of proteins are much more restrictive. We analyzed the proteome-wide data of Schwanhäusser et al. (2011) and found that 55% of the measured proteins had half-lives of <50 hr, and only 7% had half-lives of <10 hr (Figure S2B). In general, we expect that the 50 hr criterion can be used in future research as a first test to rule out circadian abundance of a molecule before more laborious experimental tests are applied (Supplemental Results; Figure S2C).

## Rhythmic Degradation Can Enhance Relative Amplitudes, Magnitudes, and Absolute Amplitudes

From the analysis above, it follows that amplitudes typically decrease in the course of biochemical reactions, due to the long half-lives of many molecular species. Increasing relative amplitudes is difficult and requires specific regulatory designs. For example, transcriptional coactivation of a transcript by a second circadian transcription factor binding to a given promoter site does not alter the relative amplitude. Doubling a sine wave doubles its magnitude as well as its absolute amplitude, and its relative amplitude remains constant. Thus, a central question is whether rhythmic degradation could boost the relative amplitude of a molecule.

The vector representation (Figure 1B) suggests that we can find a simple expression for the relative amplitude of the molecule, similar to the phase equation. This is the case, save for a correction factor $C$ (see Experimental Procedures as well):

$$A_x \approx \underbrace{\left|A_{\mathrm{prod}} e^{i\varphi_{\mathrm{prod}}} - A_{\mathrm{deg}} e^{i\varphi_{\mathrm{deg}}}\right|}_{\text{combined relative amplitude of production and degradation}} \times \underbrace{\frac{\gamma}{\sqrt{\gamma^2+\omega^2} - \frac{1}{\sqrt{\gamma^2+\omega^2}} C}}_{\text{amplitude reduction determined by mean half-life}}. \quad \text{(Equation 2)}$$

Figure 2B shows the consequences of Equation 2: rhythmic degradation enhances the relative amplitude if the degradation phase falls between 6 and 12 hr before or after the production phase. A maximal amplitude boost occurs if production and degradation are in antiphase.

In addition to phase and amplitude, the mean abundance (magnitude $M_x$) is also an important property of a circadian molecule. Rhythmic production does not change the magnitude, i.e., $M_x = k/\gamma$ as for constant production and degradation (Experimental Procedures). Surprisingly, we found that rhythmic degradation does change the magnitude (Figure 2C), which is evident in a magnitude modulation factor arising in our approximation:

$$M_x \approx \underbrace{\frac{k}{\gamma}}_{\text{non-oscillatory mean}} \times \underbrace{\frac{2(\gamma^2+\omega^2-C)}{2(\gamma^2+\omega^2)-\gamma^2 A_{\mathrm{deg}}^2}}_{\text{modulation factor}}. \quad \text{(Equation 3)}$$

Here, $C$ is the same correction term as in Equation 2 (Experimental Procedures). Thus, solely an increase of the oscillation amplitude of the half-life can result in an increase of the magnitude (switch from "a" to "b" in Figure 2C). We term this phenomenon the magnitude effect of rhythmic degradation.

Could this effect be exploited to boost circadian rhythms in transcripts or proteins? In general, significant relative amplitudes can only be obtained if the average half-lives are small (see Figure 2A), in which case also the magnitude goes down. If the magnitude is too small, even rhythms with large relative amplitudes are difficult to detect or exploit due to low-number effects and the resulting transcriptional noise (Friedman et al., 2006; Thattai and van Oudenaarden, 2001). This trade-off between sufficient magnitude and amplitude is reflected in the absolute amplitude $M_xA_x$, which measures the difference between peak and trough in the absolute abundance, i.e., in the number of molecules of a certain species.

We found that rhythmic degradation in itself increases absolute amplitudes. A given degradation amplitude causes a larger absolute amplitude in abundance than the same production amplitude would (Figure 2D). We derived a simple formula that shows that this effect only depends on the average half-life (Experimental Procedures). The effect is relevant since in practice, rhythmic signals can be best distinguished from noise if both the absolute and relative amplitudes are high. Thus, the question arises as to whether the relative amplitude can be increased without a considerable loss in absolute amplitude. We found that this is possible if the degradation is rhythmic (Figure S2D). In this case, the absolute amplitude is robust to changes in the half-life from 100 hr down to 3 hr. In this range, the relative amplitude is increased by a factor of 25 (Figure 2A). Notably, this value ($t_{1/2} \approx 3$ hr) is close to a lower bound of measured mRNA and protein half-lives (Schwanhäusser et al., 2011; Eden et al., 2011; see Figure S1B). If only production is rhythmic, the absolute amplitude is only robust to changes in the half-life down to 10 hr (Figure S2D), so that the relative amplitude can only be enhanced by a factor of 10 by a reduction in the half-life (see Figure 2A).

In summary, the present analysis reveals a largely increased plasticity induced by rhythmic production and degradation compared with rhythmic production alone. Rhythmic degradation not only dramatically increases the range of possible phases of the molecule (Figure 1C) but also enhances the average abundances and both the relative and absolute amplitudes (Figures 2B–2D).

## Rhythmic mRNA Degradation Rates Correlate with Poly(A) Tail Lengths and Interactions with Cold-Induced RNA-Binding Proteins

The mouse liver has a large circadian transcriptome, which is often thought to be the result of circadian transcriptional activities (Hughes et al., 2009). Assuming constant mRNA half-lives, transcript abundances should then be expected to have phases slightly later than the corresponding transcriptional activities, and also to have smaller relative amplitudes. However, this is partly contradicted by genome-wide studies in which transcriptional activities and mRNA abundances were both measured in mouse liver (Koike et al., 2012; Le Martelot et al., 2012; Menet

et al., 2012). These studies revealed a large group of transcripts with anomalous phase relationships between transcriptional activity and mRNA abundance. In many cases, mRNA abundances appear to peak before transcriptional activities, or transcriptional activities do not seem to be rhythmic at all, with mRNAs still exhibiting clear rhythms. It was concluded from these studies that this suggests widespread circadian posttranscriptional regulation.

We set out to precisely quantify the extent to which the circadian transcriptome is influenced by rhythmic posttranscriptional processes. To do this, we started with the genome-wide paired transcription and mRNA abundance data from Menet et al. (2012), which provide a particularly clean separation between transcriptional activity, as assayed with nascent RNA sequencing (RNA-seq) and mature mRNA abundance (assayed with poly(A)$^+$ RNA-seq). Based on the model shown in Figure 1A, we developed a chi-square test that detects disagreements between the data and the standard model of rhythmic transcription paired with constant mRNA half-lives (see Figure 3A; Experimental Procedures, and the accompanying freely available R package "patest" [File S2]). In particular, the test avoids detecting disagreements solely due to the higher level of noise in transcriptional activities (Figure 3B), which often causes standard algorithms to classify transcriptional activities as arrhythmic. For average mRNA half-lives and their standard errors, we used data from Friedel et al. (2009) and Schwanhäusser et al. (2011) (Supplemental Experimental Procedures; Figures S3A–3E). We obtained 3,027 genes for which transcriptional activity, mature mRNA abundance, and mRNA half-life data are available.

Using the accompanying R package "HarmonicRegression" (File S1), we estimated the relative amplitudes, phases, and error ellipses for nascent mRNA transcription and mature mRNA abundances, and found 1,291 mouse liver transcripts that were rhythmic in nascent and/or mature mRNA abundances, with a false discovery rate (FDR) of 25%.

We confirmed sinking relative amplitudes with longer mRNA half-lives (Experimental Procedures; Figure S3D). Our chi-square test then detected hundreds of anomalous rhythmic transcript abundances that cannot be explained by rhythmic transcription paired with constant half-lives, implying widespread posttranscriptional regulation such as rhythmic half-lives. A lower limit for the proportion of transcripts subject to rhythmic posttranscriptional control can be derived directly from the p values (Benjamini and Hochberg, 2000), leading to an estimate that at least 30% of rhythmic mouse liver transcripts are affected by rhythmic posttranscriptional regulation. Specifically, fixing the FDR at 25%, our chi-square test found 493 transcripts under rhythmic posttranscriptional regulation (Figure 3C; Table S1). Three representative examples are shown in Figure 3D, in which transcriptional activities peak either after mature mRNA abundances (for the genes *Eps8l2* and *Insig2*) or in antiphase (for the gene *Rbm3*, whose protein we return to below).

The discrepancies between measured transcriptional activities and mature mRNA abundances detected by our method could be explained by rhythmic half-lives. We computed the phases and relative amplitudes of the rhythmic degradation required to fully explain the observed nascent and mature mRNA time courses, respectively (Experimental Procedures, Equation 6; also implemented in the accompanying R package "patest" [File S2]), and obtained a phase distribution of rhythmic degradation with a peak at around ZT6, in the middle of the inactivity phase (Figure S3F).

If rhythmic degradation indeed plays a role in the mRNA abundance rhythms of the transcripts detected by our test, there should be an overrepresentation of circadian rhythms in the molecular features of mRNA that determine half-lives in this group of transcripts compared with circadian transcripts in general. One such feature is the length of the 3′ poly(A) tail, which is regulated by deadenylases (Garneau et al., 2007), including the circadian deadenylase nocturnin (Stubblefield et al., 2012). A short poly(A) tail length generally increases degradation rates. To investigate whether the poly(A) tail lengths of the transcripts detected by our method tend to be rhythmic, we analyzed data from Kojima et al. (2012). In that study, abundances of transcripts with short (60–250 nt) and long (<60 nt) poly(A) tails in mouse liver were assayed at different time points genome-wide.

Our chi-square test detected 12 rhythmic transcripts that turned out to also have rhythmic poly(A) tail lengths (Table S1). For these transcripts, phases of the predicted rhythmic degradation rates agreed well with measured times of short poly(A) tails ($p = 0.036$, circular correlation test; Figure 3E). The transcripts detected by our test were also generally strongly enriched for rhythmic poly(A) tail lengths ($p = 0.015$, Fisher's exact test; Figure 3F). Hence, mature mRNA rhythms that are not explained by rhythmic transcription rates can be partly explained by rhythmic mRNA half-lives regulated by the length of the poly(A) tail (see also discussion in Supplemental Results).

mRNA half-lives may be regulated by circadian RNA-binding proteins, such as the related cold-induced mRNA-binding proteins CIRBP and RBM3 (Morf et al., 2012; Liu et al., 2013). We compiled CIRBP–mRNA and RBM3–mRNA interaction data from these two studies and found a clear enrichment for CIRBP- and RBM3-binding transcripts among those detected by our chi-square test (Figure 3F). Thus, our chi-square test also likely detects many transcripts with rhythmic half-lives regulated by cold-induced mRNA-binding proteins.

We also tested for enrichment of targets of circadian miRNAs (Vollmers et al., 2012) as annotated in the miRTarBase database (Hsu et al., 2014), but found no significant enrichment. Although this may partly be due to incompleteness and false positives in the miRNA target annotation, it is consistent with results showing that the kinetics of miRNA–target interactions generally are too slow to play a role in circadian regulation of half-lives (Hausser et al., 2013).

The same nascent-seq and poly(A)$^+$ RNA-seq protocols were also applied in a study of *Drosophila* heads (Rodriguez et al., 2013), with results similar to those obtained in the mouse liver study (Kojima et al., 2012), i.e., nascent mRNA rhythms appeared to be noisier and a group of rhythmic transcripts showed weak or no rhythms in their nascent mRNA levels. We reanalyzed these data and found 537 transcripts with diurnal rhythms in either nascent or mature mRNA (FDR = 25%; Table S2). Together with genome-wide data for fly mRNA half-lives from Thomsen et al. (2010), we applied our chi-square test with an FDR of 0.25 and detected 109 transcripts. Since the half-life estimates are much more uncertain in this case, we used a conservative

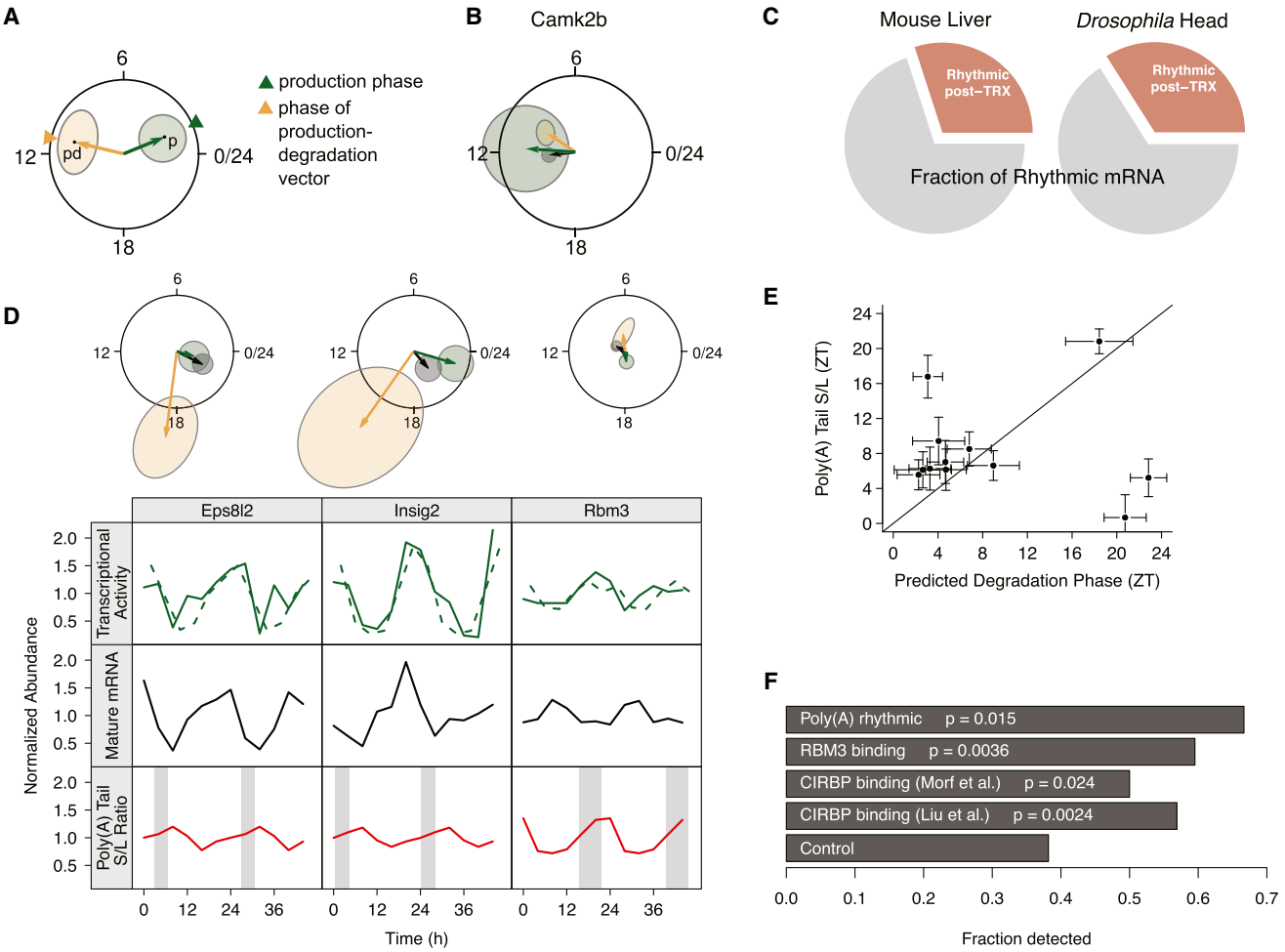


**Figure 3. Rhythmic Degradation Explains and Unifies the Observed Phase Distributions of mRNA**

(A) Illustration of the detection method. To detect transcripts affected by rhythmic posttranscriptional regulation, the relative amplitudes and phases of nascent (green, reflecting transcript production, "p") and mature mRNA abundances were estimated together with error ellipses. Mature mRNA abundances were adjusted for average transcript half-lives to yield the production-degradation (pd) vector and its error ellipse, which becomes oblong due to uncertainties in half-life measurements (Supplemental Experimental Procedures). This is the phase and relative amplitude of transcriptional activity, assuming a constant transcript half-life (orange). The normalized difference between the p and pd vectors is asymptotically chi-square distributed (Supplemental Experimental Procedures), enabling statistical testing for rhythmic posttranscriptional regulation. As a rule of thumb, statistical significance requires nonoverlapping orange and green error ellipses.

(B) With previous methods, noisy transcriptional activities may cause false positives. For the *Camk2b* transcript, standard algorithms would result in a rhythmic call for the mature mRNA but an arrhythmic call for the transcriptional activity, due to the noisy nature of the latter (large green error ellipse). Still, there is no real evidence for rhythmic posttranscriptional regulation in these data (orange and green ellipses overlap). Transcriptome-wide, the median SD of the residual after the fit (noise level) was 21% of the mean for nascent mRNA, compared with 10% for mature mRNA.

(C) Extent of rhythmic posttranscriptional regulation in mouse liver and *Drosophila* heads.

(D) Three transcripts under rhythmic posttranscriptional regulation. Top: phases, relative amplitudes, and error ellipses for nascent RNA (green) and poly(A)$^+$ mRNA (gray). The latter together with half-lives and their estimate variances yield the relative amplitudes and phases of the pd vector (orange). The transcriptional activities are nascent RNA abundances (solid curves) from Menet et al. (2012) and the polymerase II gene body occupancy measurements (dashed curves, double plotted) were obtained from Le Martelot et al. (2012). The values from Menet et al. (2012), rather than those from Le Martelot et al. (2012), were used throughout the present study due to the higher number of samples, although the agreement between the studies is excellent (Figure S3F). The ratios of short-to-long poly(A) tail lengths are from Kojima et al. (2012). Gray-shaded areas are the predicted phase ± 2 SD of the degradation rate based on the differences between the pd and p vectors (green and orange, upper panel).

(E) Predicted rhythms in degradation rates agree with measured rhythms in poly(A) tail lengths. Error bars represent approximatively ± 2 SD calculated from the error ellipses for the differences between the pd and p vectors, and from the time series of poly(A) tail lengths, respectively.

(F) Enrichment of rhythmic posttranscriptional regulators among detected transcripts. Among the 1,291 transcripts with circadian rhythms in transcriptional activities and/or mature mRNA abundances, 18 have rhythmic poly(A) tail lengths (Kojima et al., 2012), 72 bind CIRBP according to Morf et al. (2012), 58 bind CIRBP according to Liu et al. (2013), and 42 bind RBM3 (Liu et al., 2013). In each case, control represents the rest of the 1,291 circadian transcripts. Fractions represent transcripts detected by our chi-square test (e.g., 12 out of the 18 transcripts with rhythmic poly(A) tail lengths were recovered by our test, corresponding to a fraction of 0.66); p values are given for Fisher's exact test.

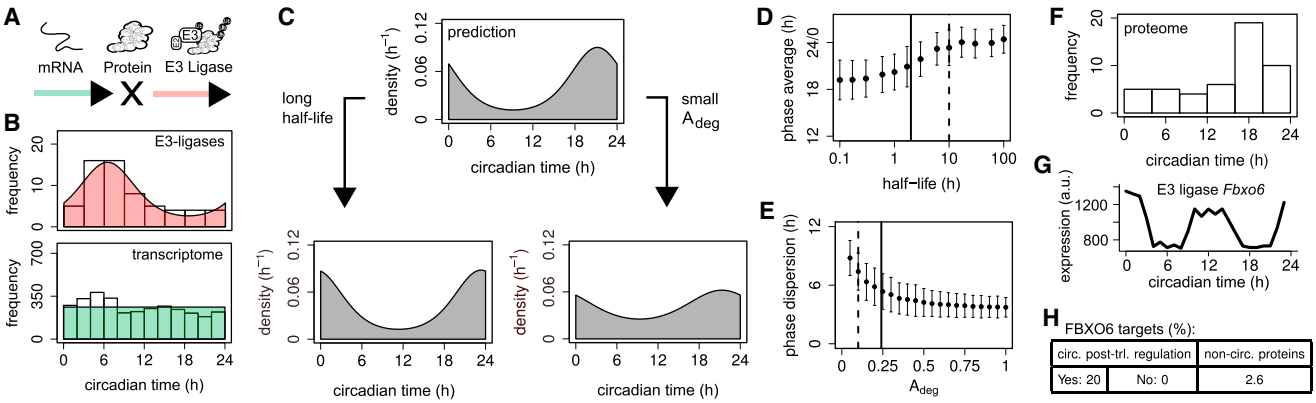


**Figure 4. The Nonuniform Phase Distribution of Protein Degradation Explains the Nonuniform Phase Distribution of the Proteome**

(A) Model scheme: proteins are produced by rhythmic mRNA and degraded by rhythmic E3 ligases.

(B) Analysis of circadian genes and ubiquitin ligase genes from Hughes et al. (2009). More than one-third of expressed E3 ligase genes are circadian ($p < 0.05$, Benjamini-Hochberg-corrected p values). The phases of circadian E3 ligase transcripts and the full circadian transcriptome, excluding E3 ligases (histograms), are distributed differently ($p < 0.01$, Watson's two-sample test) and can be described by a von Mises distribution and a circular uniform distribution, respectively (colored densities).

(C) Prediction of the phase distribution of the circadian proteome (Experimental Procedures). Parameter values: $A_{prod} = A_{deg} = 0.24$, $t_{1/2} = 2$ hr.

(D and E) Parameter dependencies of the predicted phase distribution. Top: circular average and SD. Error bars were computed by sampling normal distributions around the values for $A_{prod}$, $A_{deg}$, and $t_{1/2}$. Solid vertical lines indicate standard values used in (D), and dashed vertical lines indicate the modified values used in simulations (bottom).

(F) Phase distribution of 49 liver proteins published by Reddy et al. (2006). All phase distributions (B, C, and F) are plotted with the same density scaling.

(G and H) Circadian gene expression and analysis of targets of the ubiquitin E3 ligase FBXO6. *Fbxo6* is rhythmically translated (data in G were obtained from Jouffe et al., 2013). Circadian proteins under rhythmic posttranslational regulation are enriched for FBXO6 substrates compared with other circadian proteins (H, $p = 0.02$, Fisher's exact test, $n = 50$) or with the rest of the proteome ($p = 0.0014$, $n = 4470$).

See also Figure S4.

estimate of their variances (see Supplemental Experimental Procedures) and could still estimate that at least 34% of the fly head transcriptome is under rhythmic posttranscriptional control.

In summary, we were able to estimate a lower limit of diurnal posttranscriptional regulation in mouse liver and *Drosophila* heads: 30% and 34% of rhythmic transcripts, respectively. The transcripts detected were enriched for measured rhythmic regulators of transcript half-lives, and our model successfully predicted measured phases of rhythmic transcript poly(A) tail lengths.

## Opposite Nonuniform Phase Distributions of E3 Ligases and the Circadian Proteome

Many proteins are degraded via the ubiquitin-proteasome pathway (Clague and Urbé, 2010). E3 ligases play an important role in this pathway by binding specifically to proteins and then ubiquitinating them. We asked whether E3 ligases are rhythmic, and how such rhythmicity would shape the phase distribution of the circadian proteome. An analysis of mouse liver transcripts from Hughes et al. (2009) revealed that ~35% of all expressed E3 ligase transcripts show circadian rhythms in abundance. Moreover, we found that they have a nonuniform phase distribution with a pronounced peak around CT6, and close to a circular normal (or von Mises) distribution (Figures 4B and S4A). This is in contrast to the phase distribution of the full circadian transcriptome ($p < 0.01$, Watson's two-sample test), which is much closer to a uniform distribution.

Based on these findings and equipped with the theory derived above (Figures 1A and 1B), we sought to predict the phase distribution of the circadian proteome. For this purpose, we fixed amplitudes and average half-lives, and sampled the phases from the estimated probability distributions in Figure 4B and applied Equation 1 to infer the protein phase distribution (Figure 4C). E3 ligase activity phase is identified with the phase of E3 ligase mRNA, which is justified by the common rapid autoubiquitination of E3 ligases (de Bie and Ciechanover, 2011). In contrast to the analysis of mRNA phases above, this sampling procedure uses only the shape and peak of the phase distributions. Furthermore, it is less dependent on half-lives and amplitudes, which are difficult to measure for proteins. This approach was possible due to the characteristic shapes of the transcriptome and E3 ligase phase distributions, and necessary because E3 ligase-substrate relationships are not known at the proteome scale.

The predicted phase distribution has a pronounced maximum around CT20 and is well described by a von Mises distribution (Figures 4C and S4B). The predicted peak around CT20 is a consequence of the general properties of rhythmic half-lives captured by our model (see Figure 1B). Since the production rate (the transcriptome) has no preferred phase, the location of the protein peak is entirely determined by properties of the degradation rate coefficient. The protein peaks in antiphase to the E3 ligases (see Figure 4B), modulated by a phase shift depending on the average half-life. Longer half-lives shift the phase distribution to later circadian times (Figure 4D), whereas the phase dispersion is unchanged (Figure S4C). On the other hand, a smaller degradation amplitude causes an increased phase dispersion (Figure 4E) without changing the phase

average (Figure S4D). In the physiologic range ($t_{1/2}$ = 2 … 10 hr, $A_{deg}$ = 0.1 … 0.25; Figure S1B), the peak phase and the phase dispersion vary by less than 3 hr (Figures 4D and 4E), which shows that the predicted phase distribution is robust to uncertainty in these parameters.

For comparison, we evaluated the data of Reddy et al. (2006), which contain phase information for 49 liver proteins (Figure 4F). The histogram of those phases peaks at CT18, which is similar to our prediction. In the same study, Reddy et al. also analyzed mRNA rhythms, and found that only six out of the 49 proteins had rhythmic mRNAs, suggesting a strong role for rhythmic degradation. While our manuscript was in review, two genome-wide studies of the circadian proteome were published (Robles et al., 2014; Mauvoisin et al., 2014). The overlap between those two studies is only 14 proteins, and Reddy et al. (2006) measured an almost completely different set of proteins (Figure S4E). However, the phase distributions of all three studies are similar and are well described by our model (Figure S4F).

Our prediction for the protein phase distribution is based on the hypothesis that the circadian onset of degradation by ubiquitin E3 ligases has a marked influence on the protein phase. Although the measured phases of protein abundance are in good agreement with our theory (see above), direct experimental evidence for this hypothesis is currently not available and difficult to obtain. It would require a proteome-wide assessment in mouse liver of circadian degradation induced by ubiquitin ligases and their targets. Nevertheless, we could make specific predictions for the E3 ligase FBXO6, the targets of which have been charted in several cell types (Liu et al., 2012), and which is translated with a strong circadian rhythm (Figure 4G). We analyzed the largest circadian proteome data set to date (Mauvoisin et al., 2014), whose translational rhythms have been measured under identical conditions (Jouffe et al., 2013). Proteins whose 95% confidence interval of translational rhythms could not explain the 95% confidence interval for rhythms in abundance for any possible half-life were considered to show a strong indication of rhythmic posttranslational control (Supplemental Experimental Procedures). Interestingly, such proteins were enriched for FBXO6 targets ($p = 0.02$; Figures 4H and S4G; Table S3; Supplemental Experimental Procedures). This provides support for the notion that rhythmic E3 ligase abundances shape the phase distribution of the circadian proteome.

## DISCUSSION

Properties of the cellular circadian clock, such as feedback regulation, robustness, and cellular synchronization, have been studied carefully and successfully. Quantitative models of different complexity have been successfully used to elucidate mechanistic properties of it (Hogenesch and Ueda, 2011). However, it is still difficult to predict the consequences of circadian rhythms for cell physiology. Our approach is to analyze very simple models, also called network motifs or modules (Milo et al., 2002; Lim et al., 2013; Westermark and Herzel, 2013), that can be expected to be recurrent building blocks in cell biology. Here, we analyzed an important circadian motif: rhythmic production and degradation of a molecule. Our results complete the so-called phase-vector model, which describes the circadian output (Ukai-Tadenuma et al., 2011; Westermark and Herzel, 2013) but only considers rhythmic production rates. We found simple analytical formulae that led to a straightforward protocol for analyzing genome-wide data. By applying these methods, we could show that rhythmic degradation alone is sufficient to explain several experimental findings that seem paradoxical if only rhythmic production is accounted for. However, this does not preclude the notion that other mechanisms could cause large delays between production and abundance phases; in particular, for proteins, multistep posttranslational modifications followed by degradation provide another possible explanation.

Given our analysis, the occurrence of phase differences of more than 6 hr between production (e.g., transcription) and the produced molecule (e.g., an mRNA), or even the appearance of the product before the producer (Reddy et al., 2006; Doherty and Kay, 2012; Menet et al., 2012), is not surprising. For the case of posttranscriptional circadian regulation of the mouse liver transcriptome, we estimated conservatively that 30% of the rhythmic transcriptome is affected. Our estimate is lower than what was initially thought (Koike et al., 2012; Doherty and Kay, 2012). The initial higher estimate could partly be ascribed to higher experimental noise levels in assays of transcriptional activity, an effect that is properly taken into account by the statistical test we developed and employed here.

Our analysis predicts a phase enrichment in the evening (around CT18) for circadian proteins. This is because many E3 ligases are rhythmic with expression phases that are unusually enriched for the morning hours. This prediction corresponds well with measured phases of the circadian proteome, which indeed are enriched for evening hours (Reddy et al., 2006). Notably, autophagy, another process that contributes to protein degradation (Clague and Urbé, 2010), is also strongly circadian in mouse liver and peaks around CT6–CT9 (Ma et al., 2011), similar to what was observed for the E3 ligases. Thus, rhythmic E3 ligases and autophagy most likely play a crucial role in shaping the phase distribution of the proteome, which should be addressed in further research. We caution that we do not expect, in general, a given degradation phase to be identical to the phase of one particular E3 ligase or RNA-binding protein. Just as multiple circadian transcription factors combine to produce an effective transcription phase (Ukai-Tadenuma et al., 2011), multiple circadian RNA-binding proteins, E3 ligases (Yin et al., 2010; Yoo et al., 2013), and other factors that contribute to poly(A) tail length regulation or protein degradation likely combine to produce an effective degradation phase.

Our model is general and can be applied to a variety of biochemical motifs, such as phosphorylation-dephosphorylation cycles. One example is the phosphorylation state of the response regulator RpaA in the cyanobacterium *Synechococcus elongatus*: maximal phosphorylation of RpaA is reached 4 hr before the maximal activity of its kinase SasA (Gutu and O'Shea, 2013). Our phase-vector model (Figure 1) then predicts rhythmic dephosphorylation with a maximal rate 4 hr after the maximal phosphorylation of RpA, which was indeed measured experimentally (Gutu and O'Shea, 2013).

We found that a low average half-life (typically <10 hr; see Figures 1 and S2A) is absolutely necessary for oscillations, no

matter how strongly this half-life oscillates. A protein with a half-life oscillating wildly between 10 min and 500 hr in a circadian period will still appear virtually constant in abundance, since the average half-life is ~250 hr. A side effect of short half-lives is that they imply low mean abundances. These can be compensated for by high mean synthesis rates, but this has an additional energy cost. The magnitude effect (Figure 2) might provide an alternative to increased amplitudes. We found that rhythmic half-lives in themselves increase mean abundances without an extra bioenergetic cost. Since circadian rhythms in mammals might dampen in some peripheral tissues as animals age (Yamazaki et al., 2002), loss of rhythmic degradation may contribute to lower abundances of proteins, such as in muscle atrophy (Vinciguerra et al., 2010).

Given a moderate half-life, the strongest oscillations can be expected if production and degradation occur in antiphase, i.e., if they have a phase difference of 12 hr in a 24 hr period. Therefore, it can be advantageous if production and degradation are regulated by different parts of the circadian core clock that have different phases, emphasizing the need for a complex and diverse machinery to generate circadian rhythms in mammalian cells. This could help to elucidate the role of rhythmic degradation in the core circadian clock. For instance, the maximal activity of AMPK, which phosphorylates and destabilizes the clock protein CRY1 in mouse liver, occurs roughly in antiphase to the corresponding Cry1 mRNA abundance (Lamia et al., 2009). Our method can be applied to predict the effects of this (Figure 1): production and degradation in antiphase should lead to a maximal amplitude boost and a minimal phase-shift effect of AMPK. Consistently, smaller amplitudes but similar phases were observed in AMPK knockout mutant cells.

Many studies of biochemical processes focus on the production properties of mRNAs and proteins, but it is well known that degradation is equally important for the control of abundances (Hargrove and Schmidt, 1989; Tippmann et al., 2012), and in addition sets important properties such as the dynamic range (Hargrove and Schmidt, 1989), synchronization of pathways (Cookson et al., 2011), and the intensity of molecular noise (Thattai and van Oudenaarden, 2001). We have shown in this report that circadian control of degradation is on an equal footing with circadian production, in terms of the effect on abundances. Key properties needed for effective temporal compartmentalization, such as evolutionary decisions regarding the best phase and amplitude for a given process, can be realized by circadian regulation of production and degradation alike.

## EXPERIMENTAL PROCEDURES

### Constant Degradation

In the case of constant degradation (i.e., $A_{deg} = 0$), the model equation (Figure 1A) can be solved by standard methods (Supplemental Experimental Procedures), and in steady state we obtain a cosine curve $x(t) = M_x(1 + A_x\cos(\omega t - \varphi_x))$ with $\varphi_x = \varphi_{prod} + \arctan(\omega/\gamma)$, $A_x = A_{prod}\gamma/(\gamma^2 + \omega^2)$, $M_x = k/\gamma$.

### Analytical Approximations

We substituted the ansatz of a cosine-shaped function for the molecule $x(t)$ into the model equation (Figure 1A) and neglect terms proportional to $A_{prod}A_{deg}^2$. This is a good approximation for relative amplitudes smaller than 0.25, which applies to almost all rhythmic transcripts evaluated by harmonic regression. We then derive Equations 1 and 2, the accuracy of which we rigorously verified numerically (Supplemental Experimental Procedures; Table S4). The amplitude equation (Equation 2) contains a correction term, $C = A_{prod}A_{deg}\gamma/2 \times (\omega\sin(\varphi_{deg} - \varphi_{prod}) + \gamma\cos(\varphi_{deg} - \varphi_{prod}))$, which ensures that $A_x < A_{prod} + A_{deg}$ even for high mean degradation rate coefficients (Figure 2B). The same correction term $C$ appears in the modulation factor for the magnitude (Equation 3), but it vanishes in the absolute amplitude, which can thus be written as a linear function of product of the amplitude of the production-degradation vector:

$$M_xA_x \approx \underbrace{\left|A_{prod}e^{i\varphi_{prod}} - A_{deg}e^{i\varphi_{deg}}\right|}_{\text{amplitude of production-degradation vector}} \times \frac{k}{\sqrt{\gamma^2+\omega^2}} \times \underbrace{\frac{2(\gamma^2+\omega^2)}{2(\gamma^2+\omega^2)-\gamma^2A_{deg}^2}}_{\text{amplitude amplification}}. \quad \text{(Equation 4)}$$

We define absolute amplitude amplification by

$$\frac{[M_xA_x]_{A_{deg}>0}}{[M_xA_x]_{A_{deg}=0}} = \underbrace{\frac{2(\gamma^2+\omega^2)}{2(\gamma^2+\omega^2)-\gamma^2A_{deg}^2}}_{\text{amplitude amplification}}, \quad \text{(Equation 5)}$$

where the amplitude of the production-degradation vector is kept constant (see Figure 2D). The model can also be used to calculate the properties of rhythmic degradation when the phases and relative amplitudes of the molecule and its production rate, and the average half-life of the molecule are all given (see Figure 1B and 3A, and Supplemental Experimental Procedures for numerical verification):

$$\varphi_{deg} \approx \arg\left(A_{prod}e^{i\varphi_{prod}} - A_{pd}e^{i\varphi_{pd}}\right), \quad (6)$$

where the relative amplitude $A_{pd}$ and phase $\varphi_{pd}$ of the production-degradation vector are calculated using the half-life and the phase and relative amplitude of the molecule, yielding $A_{pd} = A_x\sqrt{\gamma^2+\omega^2}/\gamma$ and $\varphi_{pd} = \varphi_x - \arctan(\omega/\gamma)$. This procedure is implemented in the accompanying R package "patest" (File S2). Equation 6 is only valid if the correction term $C$ is small, which is the case for most observed amplitudes. Details of all the analytical calculations are given in Supplemental Experimental Procedures.

### Software and Data Analysis

Numerical computations for validation of the model and approximations were performed using custom C programs. All data analysis and processing were performed with R (R Development Core Team, 2011, http://www.r-project.org) supported by the packages developed as part of the present work ("HarmonicRegression" [File S1] and "patest" [File S2], which are described in Supplemental Experimental Procedures). Linearization and error propagation of the abundance error ellipses together with variance estimates for half-lives were used to derive the error ellipse for the production-degradation vector (Figure 3A). The difference between the production-degradation and production vectors approximately follows a 2D normal distribution with zero mean for the model with constant degradation rate coefficient, which leads to a chi-square test for this null model. The adaptive method of Benjamini and Hochberg (2000) was used to estimate the proportion of non-null p values. The E3 ligase analysis was based on microarray data (Hughes et al., 2009) under GEO accession number GSE11923. We identified circadian genes using JTK_CYCLE (Hughes et al., 2010) for a period length of 24 hr, with a cutoff of 0.05 for Benjamini-Hochberg-corrected p values, and estimated amplitudes and phases using our "HarmonicRegression" package (File S1). E3 ligases were selected by the Gene Ontology term GO:0004842 (molecular function: ubiquitin-protein ligase activity) and its descendants.

## SUPPLEMENTAL INFORMATION

Supplemental Information includes Supplemental Results, Supplemental Experimental Procedures, four figures, and four tables and can be found with this article online at http://dx.doi.org/10.1016/j.celrep.2014.09.021.

## AUTHOR CONTRIBUTIONS

S.L., K.T., and P.O.W. performed analytical and numerical calculations. S.L., P.F.T., and P.O.W. developed methods for statistical testing. P.F.T. and P.O.W analyzed data. P.F.T. and P.O.W. developed methods for statistical testing and analyzed data. P.O.W. and K.T. supervised the work and wrote the manuscript with input from S.L. and P.F.T.

## ACKNOWLEDGMENTS

We thank H. Herzel, E.D. Herzog, and A. Kramer for stimulating discussions, and K. Schellenberg and S. Hertel for critical readings of the manuscript. This study was supported by the BMBF (FKZ 0315899, GerontoSys).

Received: July 10, 2013
Revised: July 4, 2014
Accepted: September 11, 2014
Published: October 16, 2014

## REFERENCES

Asher, G., and Schibler, U. (2011). Crosstalk between components of circadian and metabolic cycles in mammals. Cell Metab. *13*, 125–137.

Baggs, J.E., and Green, C.B. (2003). Nocturnin, a deadenylase in Xenopus laevis retina: a mechanism for posttranscriptional control of circadian-related mRNA. Curr. Biol. *13*, 189–198.

Bass, J., and Takahashi, J.S. (2010). Circadian integration of metabolism and energetics. Science *330*, 1349–1354.

Benjamini, Y., and Hochberg, Y. (2000). On the adaptive control of the false discovery rate in multiple testing with independent statistics. J. Educ. Behav. Stat. *25*, 60–83.

Clague, M.J., and Urbé, S. (2010). Ubiquitin: same molecule, different degradation pathways. Cell *143*, 682–685.

Cookson, N.A., Mather, W.H., Danino, T., Mondragón-Palomino, O., Williams, R.J., Tsimring, L.S., and Hasty, J. (2011). Queueing up for enzymatic processing: correlated signaling through coupled degradation. Mol. Syst. Biol. *7*, 561.

de Bie, P., and Ciechanover, A. (2011). Ubiquitination of E3 ligases: self-regulation of the ubiquitin system via proteolytic and non-proteolytic mechanisms. Cell Death Differ. *18*, 1393–1402.

Doherty, C.J., and Kay, S.A. (2010). Circadian control of global gene expression patterns. Annu. Rev. Genet. *44*, 419–444.

Doherty, C.J., and Kay, S.A. (2012). Circadian surprise—it's not all about transcription. Science *338*, 338–340.

Eden, E., Geva-Zatorsky, N., Issaeva, I., Cohen, A., Dekel, E., Danon, T., Cohen, L., Mayo, A., and Alon, U. (2011). Proteome half-life dynamics in living human cells. Science *331*, 764–768.

Friedel, C.C., Dölken, L., Ruzsics, Z., Koszinowski, U.H., and Zimmer, R. (2009). Conserved principles of mammalian transcriptional regulation revealed by RNA half-life. Nucleic Acids Res. *37*, e115.

Friedman, N., Cai, L., and Xie, X.S. (2006). Linking stochastic dynamics to population distribution: an analytical framework of gene expression. Phys. Rev. Lett. *97*, 168302.

Garneau, N.L., Wilusz, J., and Wilusz, C.J. (2007). The highways and byways of mRNA decay. Nat. Rev. Mol. Cell Biol. *8*, 113–126.

Gutu, A., and O'Shea, E.K. (2013). Two antagonistic clock-regulated histidine kinases time the activation of circadian gene expression. Mol. Cell *50*, 288–294.

Hargrove, J.L., and Schmidt, F.H. (1989). The role of mRNA and protein stability in gene expression. FASEB J. *3*, 2360–2370.

Hausser, J., Syed, A.P., Selevsek, N., van Nimwegen, E., Jaskiewicz, L., Aebersold, R., and Zavolan, M. (2013). Timescales and bottlenecks in miRNA-dependent gene regulation. Mol. Syst. Biol. *9*, 711.

Hogenesch, J.B., and Ueda, H.R. (2011). Understanding systems-level properties: timely stories from the study of clocks. Nat. Rev. Genet. *12*, 407–416.

Hsu, S.-D., Tseng, Y.-T., Shrestha, S., Lin, Y.-L., Khaleel, A., Chou, C.-H., Chu, C.-F., Huang, H.-Y., Lin, C.-M., Ho, S.-Y., et al. (2014). miRTarBase update 2014: an information resource for experimentally validated miRNA-target interactions. Nucleic Acids Res. *42*, D78–D85.

Hughes, M.E., DiTacchio, L., Hayes, K.R., Vollmers, C., Pulivarthy, S., Baggs, J.E., Panda, S., and Hogenesch, J.B. (2009). Harmonics of circadian gene transcription in mammals. PLoS Genet. *5*, e1000442.

Hughes, M.E., Hogenesch, J.B., and Kornacker, K. (2010). JTK_CYCLE: an efficient nonparametric algorithm for detecting rhythmic components in genome-scale data sets. J. Biol. Rhythms *25*, 372–380.

Jouffe, C., Cretenet, G., Symul, L., Martin, E., Atger, F., Naef, F., and Gachon, F. (2013). The circadian clock coordinates ribosome biogenesis. PLoS Biol. *11*, e1001455.

Koike, N., Yoo, S.-H., Huang, H.-C., Kumar, V., Lee, C., Kim, T.-K., and Takahashi, J.S. (2012). Transcriptional architecture and chromatin landscape of the core circadian clock in mammals. Science *338*, 349–354.

Kojima, S., Shingle, D.L., and Green, C.B. (2011). Post-transcriptional control of circadian rhythms. J. Cell Sci. *124*, 311–320.

Kojima, S., Sher-Chen, E.L., and Green, C.B. (2012). Circadian control of mRNA polyadenylation dynamics regulates rhythmic protein expression. Genes Dev. *26*, 2724–2736.

Lamia, K.A., Sachdeva, U.M., DiTacchio, L., Williams, E.C., Alvarez, J.G., Egan, D.F., Vasquez, D.S., Juguilon, H., Panda, S., Shaw, R.J., et al. (2009). AMPK regulates the circadian clock by cryptochrome phosphorylation and degradation. Science *326*, 437–440.

Le Martelot, G., Canella, D., Symul, L., Migliavacca, E., Gilardi, F., Liechti, R., Martin, O., Harshman, K., Delorenzi, M., Desvergne, B., et al.; CycliX Consortium (2012). Genome-wide RNA polymerase II profiles and RNA accumulation reveal kinetics of transcription and associated epigenetic changes during diurnal cycles. PLoS Biol. *10*, e1001442.

Lim, W.A., Lee, C.M., and Tang, C. (2013). Design principles of regulatory networks: searching for the molecular algorithms of the cell. Mol. Cell *49*, 202–212.

Liu, B., Zheng, Y., Wang, T.-D., Xu, H.-Z., Xia, L., Zhang, J., Wu, Y.-L., Chen, G.Q., and Wang, L.-S. (2012). Proteomic identification of common SCF ubiquitin ligase FBXO6-interacting glycoproteins in three kinds of cells. J. Proteome Res. *11*, 1773–1781.

Liu, Y., Hu, W., Murakawa, Y., Yin, J., Wang, G., Landthaler, M., and Yan, J. (2013). Cold-induced RNA-binding proteins regulate circadian gene expression by controlling alternative polyadenylation. Sci. Rep. *3*, 2054.

Ma, D., Panda, S., and Lin, J.D. (2011). Temporal orchestration of circadian autophagy rhythm by C/EBP$\beta$. EMBO J. *30*, 4642–4651.

Matsuo, T., Yamaguchi, S., Mitsui, S., Emi, A., Shimoda, F., and Okamura, H. (2003). Control mechanism of the circadian clock for timing of cell division in vivo. Science *302*, 255–259.

Mauvoisin, D., Wang, J., Jouffe, C., Martin, E., Atger, F., Waridel, P., Quadroni, M., Gachon, F., and Naef, F. (2014). Circadian clock-dependent and -independent rhythmic proteomes implement distinct diurnal functions in mouse liver. Proc. Natl. Acad. Sci. USA *111*, 167–172.

Menet, J.S., Rodriguez, J., Abruzzi, K.C., and Rosbash, M. (2012). Nascent-Seq reveals novel features of mouse circadian transcriptional regulation. eLife *1*, e00011.

Milo, R., Shen-Orr, S., Itzkovitz, S., Kashtan, N., Chklovskii, D., and Alon, U. (2002). Network motifs: simple building blocks of complex networks. Science *298*, 824–827.

Morf, J., Rey, G., Schneider, K., Stratmann, M., Fujita, J., Naef, F., and Schibler, U. (2012). Cold-inducible RNA-binding protein modulates circadian gene expression posttranscriptionally. Science *338*, 379–383.

Reddy, A.B., Karp, N.A., Maywood, E.S., Sage, E.A., Deery, M., O'Neill, J.S., Wong, G.K., Chesham, J., Odell, M., Lilley, K.S., et al. (2006). Circadian orchestration of the hepatic proteome. Curr. Biol. *16*, 1107–1115.

Robinson, B.G., Frim, D.M., Schwartz, W.J., and Majzoub, J.A. (1988). Vasopressin mRNA in the suprachiasmatic nuclei: daily regulation of polyadenylate tail length. Science *241*, 342–344.

Robles, M.S., Cox, J., and Mann, M. (2014). In-vivo quantitative proteomics reveals a key contribution of post-transcriptional mechanisms to the circadian regulation of liver metabolism. PLoS Genet. *10*, e1004047.

Rodriguez, J., Tang, C.-H.A., Khodor, Y.L., Vodala, S., Menet, J.S., and Rosbash, M. (2013). Nascent-Seq analysis of Drosophila cycling gene expression. Proc. Natl. Acad. Sci. USA *110*, E275–E284.

Schwanhäusser, B., Busse, D., Li, N., Dittmar, G., Schuchhardt, J., Wolf, J., Chen, W., and Selbach, M. (2011). Global quantification of mammalian gene expression control. Nature *473*, 337–342.

Stubblefield, J.J., Terrien, J., and Green, C.B. (2012). Nocturnin: at the crossroads of clocks and metabolism. Trends Endocrinol. Metab. *23*, 326–333.

Thattai, M., and van Oudenaarden, A. (2001). Intrinsic noise in gene regulatory networks. Proc. Natl. Acad. Sci. USA *98*, 8614–8619.

Thomsen, S., Anders, S., Janga, S.C., Huber, W., and Alonso, C.R. (2010). Genome-wide analysis of mRNA decay patterns during early Drosophila development. Genome Biol. *11*, R93.

Tippmann, S.C., Ivanek, R., Gaidatzis, D., Schöler, A., Hoerner, L., van Nimwegen, E., Stadler, P.F., Stadler, M.B., and Schübeler, D. (2012). Chromatin measurements reveal contributions of synthesis and decay to steady-state mRNA levels. Mol. Syst. Biol. *8*, 593.

Ukai-Tadenuma, M., Yamada, R.G., Xu, H., Ripperger, J.A., Liu, A.C., and Ueda, H.R. (2011). Delay in feedback repression by cryptochrome 1 is required for circadian clock function. Cell *144*, 268–281.

Vinciguerra, M., Musaro, A., and Rosenthal, N. (2010). Regulation of muscle atrophy in aging and disease. Adv. Exp. Med. Biol. *694*, 211–233.

Vollmers, C., Schmitz, R.J., Nathanson, J., Yeo, G., Ecker, J.R., and Panda, S. (2012). Circadian oscillations of protein-coding and regulatory RNAs in a highly dynamic mammalian liver epigenome. Cell Metab. *16*, 833–845.

Westermark, P.O., and Herzel, H. (2013). Mechanism for 12 hr rhythm generation by the circadian clock. Cell Reports *3*, 1228–1238.

Woo, K.-C., Ha, D.-C., Lee, K.-H., Kim, D.-Y., Kim, T.-D., and Kim, K.-T. (2010). Circadian amplitude of cryptochrome 1 is modulated by mRNA stability regulation via cytoplasmic hnRNP D oscillation. Mol. Cell. Biol. *30*, 197–205.

Yamazaki, S., Straume, M., Tei, H., Sakaki, Y., Menaker, M., and Block, G.D. (2002). Effects of aging on central and peripheral mammalian clocks. Proc. Natl. Acad. Sci. USA *99*, 10801–10806.

Yin, L., Joshi, S., Wu, N., Tong, X., and Lazar, M.A. (2010). E3 ligases Arf-bp1 and Pam mediate lithium-stimulated degradation of the circadian heme receptor Rev-erb alpha. Proc. Natl. Acad. Sci. USA *107*, 11614–11619.

Yoo, S.-H., Mohawk, J.A., Siepka, S.M., Shan, Y., Huh, S.K., Hong, H.-K., Kornblum, I., Kumar, V., Koike, N., Xu, M., et al. (2013). Competing E3 ubiquitin ligases govern circadian periodicity by degradation of CRY in nucleus and cytoplasm. Cell *152*, 1091–1105.

Zhang, E.E., and Kay, S.A. (2010). Clocks not winding down: unravelling circadian networks. Nat. Rev. Mol. Cell Biol. *11*, 764–776.